

Three-integral models for axisymmetric galactic discs

B. Famaey¹, K. Van Caelenberg² and H. Dejonghe²

¹*Institut d’Astronomie et d’Astrophysique CP226, Université Libre de Bruxelles, Boulevard du Triomphe, B-1050 Bruxelles, Belgium. Ph.D. student F.R.I.A., E-mail: bfamaey@astro.ulb.ac.be*

²*Sterrenkundig Observatorium, Universiteit Gent, Krijgslaan 281, B-9000 Gent, Belgium*

Accepted ... Received 2001 december

ABSTRACT

We present new equilibrium component distribution functions that depend on three analytic integrals in a Stäckel potential, and that can be used to model stellar discs of galaxies. These components are generalizations of two-integral ones and can thus provide thin discs in the two-integral approximation. Their most important properties are the partly analytical expression for their moments, the disc-like features of their configuration space densities (exponential decline in the galactic plane and finite extent in the vertical direction) and the anisotropy of their velocity dispersions. We further show that a linear combination of such components can fit a van der Kruit disc.

Key words:

galaxies: kinematics and dynamics – galaxies: structure – stars: kinematics.

1 INTRODUCTION

It has been known for a long time that the classical two-integral equilibrium theory in axisymmetric geometry is not sufficient to adequately describe the stellar discs of galaxies. In accordance with Jeans theorem (Jeans 1915), the phase space distribution function of a stellar system in a steady state depends only on the isolating integrals of the motion; the binding energy E and the vertical component of the angular momentum L_z are isolating integrals in a stationary and axisymmetric system. It is a fundamental property of all two-integral distribution functions $F(E, L_z)$ that the dispersion of the velocity in the radial direction equals the dispersion in the vertical direction: we know that, for example, the disc of the Milky Way does not have that property (Binney & Merrifield 1998). Illustrations of other shortcomings of a two-integral model in a galactic context can be found in Durand, Dejonghe & Acker (1996).

The introduction of a third integral of the motion helps to overcome these constraints: in that case, the velocity dispersions can be different in all the directions. Numerical experiments show that a third isolating integral seems to exist for most orbits in realistic galactic potentials (Ollongren 1962, Innanen & Papp 1977, Richstone 1982). This third integral can be taken into account numerically in the models by using extensions of Schwarzschild’s (1979) orbit superposition technique (Cretton et al. 1999, Zhao 1999, Häfner et al. 2000). It is also possible to define an analytic third integral specific to particular orbital families (de Zeeuw, Evans & Schwarzschild 1996, Evans, Häfner & de Zeeuw 1997) or an approximate global third integral (Petrou 1983ab, Dehnen & Gerhard 1993), but we choose to construct models with an exact analytic third integral by using a Stäckel potential (Stäckel 1890, de Zeeuw 1985).

It is not quite obvious to define suitable global distribution functions $F(E, L_z, I_3)$ that depend on three exact analytic integrals and that can somewhat realistically represent our ideas of a real stellar disc. For example, Bienaymé (1999) made three-integral extensions of the two-integral parametric distribution functions described in Bienaymé & Séchaud (1997), but these ones were built to model the kinematics of neighbouring stars in the Milky Way only. Dejonghe & Laurent (1991) also defined the three-integral Abel distribution functions, but these ones could not provide very thin discs in the two-integral approximation. Robijn & de Zeeuw (1996) constructed three-integral distribution functions for oblate galaxy models, but they also had problems to recover the two-integral approximation.

In this paper we continue the work of Batsleer & Dejonghe (1995), who constructed component distribution functions that are two-integral, but that can represent (very) thin discs when a judicious linear combination of them is chosen. We use these components as a basis for new component distribution functions that are three-integral, of which the Batsleer & Dejonghe components are a special case.

In the next section, we outline some fundamentals of two-integral equilibrium systems and we show how to model discs with a finite extent in the vertical direction. In section 3, we present some general facts about Stäckel potentials and we present new analytic three-integral distribution functions that can represent stellar discs. An analytical expression for the moments of these distribution functions is calculated in section 4. In the next section, we discuss their physical properties and

show their realistic disc-like character. Finally, in section 6, we show that these distribution functions can be used as basis functions in the modeling of a van der Kruit disc. For the conclusions, we refer to section 7.

2 TWO-INTEGRAL FUNDAMENTALS

We denote the gravitational potential in cylindrical coordinates (ϖ, ϕ, z) by $V(\varpi, z) = -\psi(\varpi, z) \leq 0$. The two classical isolating integrals of the motion are the binding energy, $E = \psi(\varpi, z) - \frac{1}{2}v^2$, and the z -component of the angular momentum, $L_z = \varpi v_\phi = \varpi^2 \dot{\phi}$.

When we use the term orbit, we do not consider the information contained in the phases of the orbital motion: an orbit is thus shorthand for an orbital density. Even with this definition, each pair (E, L_z) represents a family of orbits; to uniquely identify one particular orbit, we need the presence of a third effective integral of the motion (i.e. we need a triple (E, L_z, I_3)).

The axisymmetric nature of the system implies we can focus on the motion in a meridional plane (i.e. a plane with constant ϕ). For a position (ϖ_0, z_0) in the meridional plane, the expressions for E and L_z imply that all families of orbits that visit this position have isolating integrals of the motion (E, L_z) that meet the requirement

$$E \leq \psi(\varpi_0, z_0) - \frac{L_z^2}{2\varpi_0^2}, \quad (1)$$

since we know that

$$v_\varpi^2 + v_z^2 \geq 0. \quad (2)$$

For given E and L_z , this relation restricts possible motion for the corresponding family of orbits to a toroidal volume in configuration space.

In (E, L_z) -space, Eq. (1) defines the region in which the points correspond to families of orbits passing through (ϖ_0, z_0) . The boundary line (equality in Eq. (1)) contains orbits that reach the given position with zero velocity (2) in the meridional plane. Keeping $z = z_0$ fixed while allowing ϖ to vary then gives us a family of such boundary lines, of which we denote the envelope by

$$E = S_{z_0}(L_z), \quad (3)$$

with the parametric equations (Batsleer & Dejonghe 1995, Eq. 4 & 5)

$$\begin{cases} E &= \psi(\varpi, z_0) - \frac{L_z^2}{2\varpi^2} \\ L_z^2 &= -\varpi^3 \frac{\partial \psi}{\partial \varpi}(\varpi, z_0). \end{cases} \quad (4)$$

All points in integral space with $E < S_{z_0}(L_z)$ represent families of orbits that will pass through $z = z_0$ at a certain ϖ . Orbits for which $E = S_{z_0}(L_z)$ also do reach the height z_0 , but can never go any higher. All points in integral space with $E > S_{z_0}(L_z)$ represent families of orbits that cannot reach $z = z_0$. S_{z_0} is thus the minimal binding energy of an orbit that cannot bring a star higher than z_0 above the galactic plane.

For every height $z_1 > z_0$ we find a similar curve $E = S_{z_1}(L_z)$, with $S_{z_1}(L_z) < S_{z_0}(L_z)$ for every value of L_z . Similarly, the envelope for the orbits that cannot go higher than $z = 0$ is given by $E = S_0(L_z)$, which gives us all circular orbits in the galactic plane.

Orbits belonging to a disc with a maximum height z_0 are thus given by (E, L_z) for which $S_{z_0}(L_z) \leq E \leq S_0(L_z)$ (the shaded area in Figure 1). Batsleer & Dejonghe (1995) constructed disc-like component distribution functions with a finite extent in vertical direction by setting them equal to zero for $E < S_{z_0}(L_z)$. In order to fully understand the components that we present here, that paper should probably be considered as preparatory reading.

3 CONSTRUCTION OF THREE-INTEGRAL COMPONENTS

3.1 Spheroidal coordinates and Stäckel potentials

We will work in *spheroidal coordinates*, since these coordinates allow a simple expression for our (axisymmetric) Stäckel potential. Spheroidal coordinates are given by (λ, ϕ, ν) , with λ and ν the roots for τ of

$$\frac{\varpi^2}{\tau + \alpha} + \frac{z^2}{\tau + \gamma} = 1 \quad \alpha < \gamma < 0, \quad (5)$$

and (ϖ, ϕ, z) cylindrical coordinates. The parameters α and γ are both constant and smaller than zero.

A potential is of *Stäckel form*, if there exists a spheroidal coordinate system (λ, ϕ, ν) , in which the potential can be written as

$$V(\lambda, \nu) = -\frac{f(\lambda) - f(\nu)}{\lambda - \nu}, \quad (6)$$

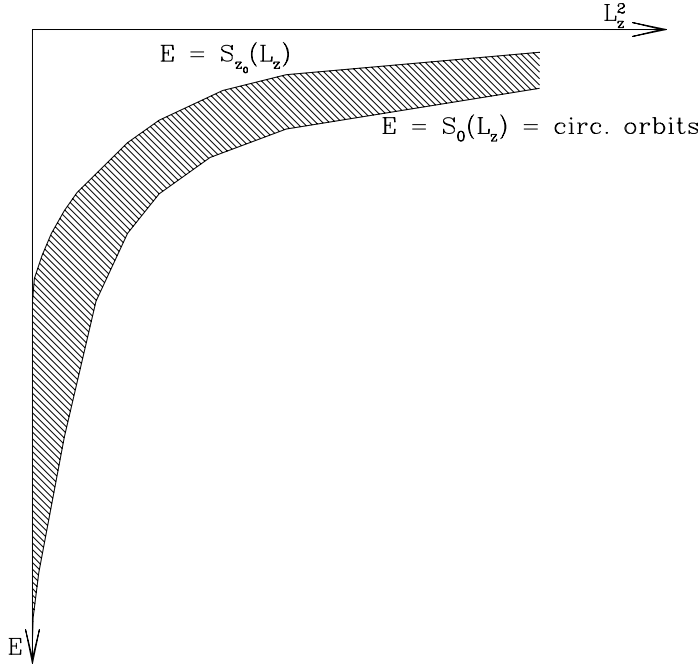


Figure 1. The shaded area is the area in the (E, L_z^2) -plane for which the corresponding families of orbits cannot go higher than z_0 above the galactic plane. The distribution function of a stellar disc with maximum height z_0 is null outside of this area.

for an arbitrary function $f(\tau) = (\tau + \gamma)G(\tau)$, $\tau = \lambda, \nu$. The function $-G(\lambda)$ then represents the potential in the $z = 0$ plane.

For this kind of potential, the Hamilton-Jacobi equation is separable in spheroidal coordinates, and therefore the orbits admit three analytic isolating integrals of the motion. The third integral of galactic dynamics has the form

$$I_3 = \frac{1}{2}(L_x^2 + L_y^2) + (\gamma - \alpha) \left[\frac{1}{2}v_z^2 - z^2 \frac{G(\lambda) - G(\nu)}{\lambda - \nu} \right] \quad (7)$$

More details can be found in de Zeeuw (1985) and in Dejonghe & de Zeeuw (1988).

3.2 Modified Fricke components

As mentioned before, we intend to create three-integral stellar distribution functions, for the construction of stellar discs: we want to achieve an exponential decline in the mass density for large radii, while we want to introduce a preference for (almost) circular orbits.

It has been known for some time that two-integral models can describe very thin disc systems, with the restriction that both vertical and radial dispersions are equal (Jarvis & Freeman 1985). So we want to create three-integral distribution functions that can describe very thin discs in the two-integral approximation, unlike the Abel distribution functions (Dejonghe & Laurent 1991).

The Fricke components (Fricke 1952) $E^\eta L_z^\beta$ favour that part of phase space where stars populate circular orbits, so they could be taken as a starting point. However, they cannot be used in their basic form to model discs with a finite extent because they populate orbits which can reach arbitrary large heights: therefore, we will take as a starting point the components defined in Batsleer & Dejonghe (1995, Eq. 19).

In order to make the components depending on the third integral I_3 , we introduce the factor $(p + qE + rL_z^2 + sI_3)^\delta$ in which the parameter s (and δ) will be responsible for the three-integral character of the components. The coefficients p , q , r and s can, in the most general case, be functions of L_z .

This leads us towards a general three-integral disc component of the form

$$F(E, L_z, I_3) = f(L_z) \left(\frac{E - S_{z_0}(L_z)}{S_0(L_z) - S_{z_0}(L_z)} \right)^\eta (p + qE + rL_z^2 + sI_3)^\delta \quad (8)$$

if

$$\begin{cases} E - S_{z_0}(L_z) \geq 0 \\ p + qE + rL_z^2 + sI_3 \geq 0 \end{cases} \quad (9)$$

The distribution function is identically zero in all other cases. The function $f(L_z)$ is defined as

$$f(L_z) = \frac{1}{1 + e^{-aL_z}} (2L_z^2 S_{z_0}(L_z))^\beta (S_{z_0}(L_z))^{\alpha_1} e^{-\frac{\alpha_2}{S_{z_0}(L_z)}}. \quad (10)$$

The parameter a is the rotation parameter (the value of a influences only the odd moments of F , see section 4). If $a = 0$, there is no rotation for the component, and if $a = +\infty$, F represents a *maximum streaming* component with no counter-rotating stars.

The requested exponential decline in the mass density with large radii is controlled by the parameter α_2 (and to some extent by the parameter α_1 , see section 5).

The parameter η is responsible for the favouring of almost circular orbits, i.e. orbits with a binding energy E as close as possible to that of circular orbits in the galactic plane (see section 5).

Furthermore, if we want to favour (almost) circular orbits, we have to suppose the distribution function to be an increasing function of E : this forces q to be positive.

Since a large I_3 implies that the orbit can reach a large height above the galactic plane (see de Zeeuw 1985 for a complete analysis of the orbits in a Stäckel potential), the orbits with small I_3 's have to be favoured in order to describe thin discs: this forces s to be negative.

Other constraints (on p , q , r , s and η) will be imposed in section 4, in order to enable the analytical calculations of the moments.

4 MOMENTS

4.1 Theory

The moments of a distribution function F at the point (λ, ϕ, ν) of a spheroidal coordinate system are defined as

$$\mu_{l,m,n}(\lambda, \nu) = \iiint F(E, L_z, I_3) v_\lambda^l v_\phi^m v_\nu^n dv_\lambda dv_\phi dv_\nu, \quad (11)$$

with v_λ , v_ϕ , v_ν the components of the velocity in the λ , the ϕ and the ν direction of the spheroidal coordinate system, and l , m , n integers.

The mass density, the mean velocity and the velocity dispersions of the stellar system represented by F can easily be expressed in terms of the moments (11) by

$$\begin{aligned} \rho(\lambda, \nu) &= \mu_{0,0,0}(\lambda, \nu) \\ \rho\langle v_\phi \rangle(\lambda, \nu) &= \mu_{0,1,0}(\lambda, \nu) \\ \rho\sigma_\lambda^2(\lambda, \nu) &= \mu_{2,0,0}(\lambda, \nu) \\ \rho\langle v_\phi^2 \rangle(\lambda, \nu) &= \mu_{0,2,0}(\lambda, \nu) \\ \rho\sigma_\nu^2(\lambda, \nu) &= \mu_{0,0,2}(\lambda, \nu) \end{aligned} \quad (12)$$

To obtain the value of one of these moments, we have to integrate over the volume in velocity-space corresponding to all orbits that pass through the point (λ, ϕ, ν) .

Since all three integrals of the motion are quadratic in v_λ and v_ν , if l or n is an odd integer, the moment $\mu_{l,m,n}$ is identically zero. If l and n are even integers, the moment $\mu_{l,m,n}$ can be written as an integral computed in the integral space. We assume in sections 4.1 and 4.2 that $a = 0$ (in that case, there is no rotation and if m is odd, the moment is zero) and that m is an even integer (the general case will easily be derived from this one in section 4.3). Under these assumptions,

$$\mu_{l,m,n} = \frac{2^{\frac{l+n}{2}+1}}{\varpi(\lambda - \nu)^{\frac{l+n}{2}}} \int \frac{f(L_z^2)}{\sqrt{L_z^2}} v_\phi^m dL_z^2 \int \int dE dI_3 \left(\frac{E - S_{z_0}}{S_0 - S_{z_0}} \right)^\eta (p + qE + rL_z^2 + sI_3)^\delta (I_3^+ - I_3)^{\frac{l-1}{2}} (I_3 - I_3^-)^{\frac{n-1}{2}} \quad (13)$$

where I_3^+ and I_3^- are given by

$$\begin{cases} I_3^+(E, L_z^2) = (\lambda + \gamma)[G(\lambda) - E] - \frac{\lambda + \gamma}{2(\lambda + \alpha)} L_z^2 \\ I_3^-(E, L_z^2) = (\nu + \gamma)[G(\nu) - E] - \frac{\nu + \gamma}{2(\nu + \alpha)} L_z^2. \end{cases} \quad (14)$$

More details can be found in Dejonghe & de Zeeuw (1988).

For our components given by Equation (8), the integration surface in the (E, I_3) -plane is defined by

$$\begin{cases} I_3^-(E, L_z^2) \leq I_3 \leq I_3^+(E, L_z^2) \\ S_{z_0}(L_z) \leq E \leq \psi - \frac{L_z^2}{2\varpi^2} \\ p + qE + rL_z^2 + sI_3 \geq 0. \end{cases} \quad (15)$$

The integration limits for the integral in L_z^2 will be determined in section 4.3.

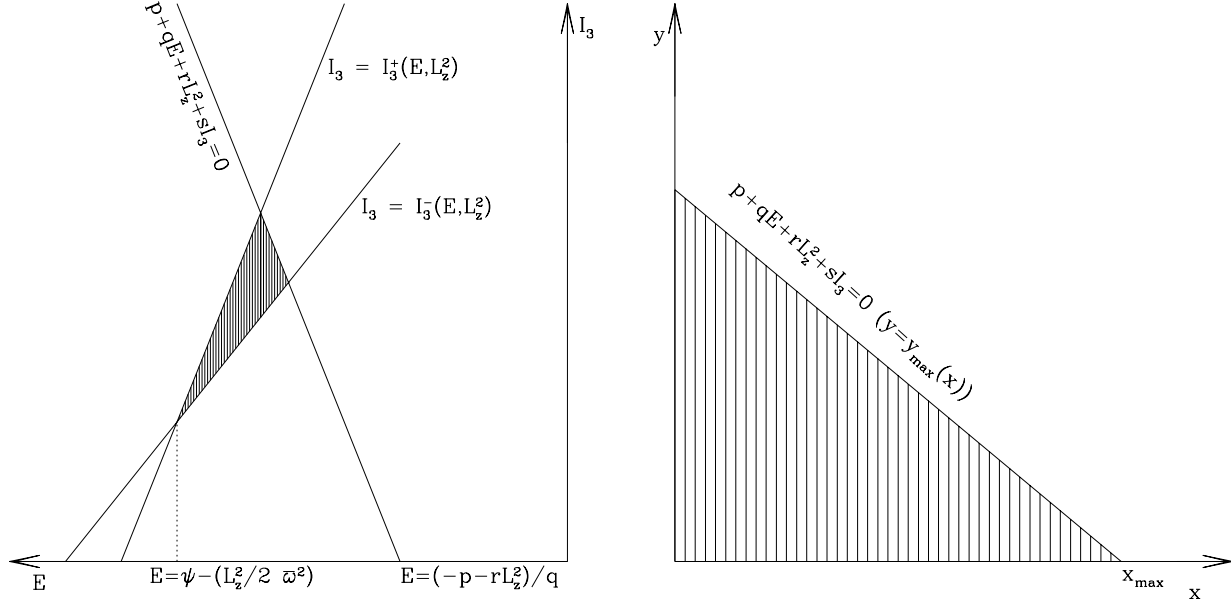


Figure 2. The integration area for the inner double integral in Equation (13) in the (E, I_3) -plane (left panel, L_z is fixed) and in the $(x(E, I_3), y(E, I_3))$ -plane (right panel, see Equation 19).

4.2 (Partly) Analytical expression for the moments

We want to reduce the triple integral (13) to a simple one by solving the innermost double integral analytically. The reader not interested in the mathematical details might step directly to section 5.

For this double integral to be analytically solved, however, we will have to make use of those combinations of p , q , r and s (see section 4.3) for which the integration area is transformed into the triangle bounded by

$$\begin{cases} I_3 = I_3^+(E, L_z^2) \\ I_3 = I_3^-(E, L_z^2) \\ p + qE + rL_z^2 + sI_3 = 0, \end{cases} \quad (16)$$

as shown in Figure 2. In this situation, we can express the factor $(E - S_{z0})/(S_0 - S_{z0})$ as a linear combination of the other three factors in the integrand (corresponding to the bounding lines of the integration surface):

$$\frac{E - S_{z0}}{S_0 - S_{z0}} = t(I_3^+ - I_3) + u(I_3 - I_3^-) + v(p + qE + rL_z^2 + sI_3). \quad (17)$$

We impose η to be an integer: then the double integral in the (E, I_3) -plane transforms into a sum of integrals:

$$\sum_{i=0}^{\eta} \sum_{j=0}^{\eta-i} \binom{\eta}{i} \binom{\eta-i}{j} v^i t^{\eta-i-j} u^j \int \int dE dI_3 (p + qE + rL_z^2 + sI_3)^{\delta+i} (I_3^+ - I_3)^{\eta + \frac{L_z^2}{2} - i - j} (I_3 - I_3^-)^{\frac{\eta-1}{2} + j} \quad (18)$$

For each integral in this summation, the integrand consists of factors whose zero-points define the bounding lines for the integration surface in the (E, I_3) -plane. These integrals can be solved analytically.

We will be in this situation (for all the points (λ, ϕ, ν) of configuration space, where the moments are calculated) whenever $p + qE + rL_z^2 + sI_3 = 0$ does intersect the E -axis for $E \geq S_{z0}(L_z)$.

In order to solve the integrals analytically, one uses the new integration variables x and y , defined by (for a fixed L_z)

$$\begin{cases} x(E, I_3) = I_3^+(E) - I_3 \\ y(E, I_3) = I_3 - I_3^-(E). \end{cases} \quad (19)$$

The line in the (E, I_3) -plane $p + qE + rL_z^2 + sI_3 = 0$ becomes $y = y_{\max}(x)$, and the root of $y_{\max}(x) = 0$ is x_{\max} (see Figure 2). To make a more compact notation possible, we first define the auxiliary functions $g(\tau)$ and $h(\tau)$, as

$$g(\tau) = G(\tau) - \frac{L_z^2}{2(\tau + \alpha)} \quad (20)$$

and

$$h(\tau) = s(\tau + \gamma) - q. \quad (21)$$

We then have

$$x_{\max} = - \left\{ p + rL_z^2 - h(\nu)\psi(\lambda, \nu) + s(\nu + \gamma)G(\nu) - \frac{L_z^2}{2\varpi^2}(q - sz^2) \right\} \frac{(\lambda - \nu)}{h(\nu)} \quad (22)$$

$$\equiv - \frac{(\lambda - \nu)}{h(\nu)} x'_{\max} \quad (23)$$

and

$$y_{\max}(x) = \frac{h(\nu)}{h(\lambda)} (x_{\max} - x) \quad (24)$$

Solving the integral part of one of the terms in Eq. (18) for y then yields

$$\begin{aligned} & \frac{1}{(\lambda - \nu)^{\delta+i+1}} \int_0^{x_{\max}} x^{\eta + \frac{l-1}{2} - i - j} dx \int_0^{y_{\max}(x)} y^{\frac{n-1}{2} + j} [h(\lambda)(y - y_{\max}(x))]^{\delta+i} dy \\ &= \frac{(-h(\lambda))^{\delta+i}}{(\lambda - \nu)^{\delta+i+1}} B\left(\frac{n-1}{2} + j + 1, \delta + i + 1\right) \int_0^{x_{\max}} x^{\eta + \frac{l-1}{2} - i - j} y_{\max}(x)^{\frac{n-1}{2} + i + j + \delta + 1} dx \end{aligned} \quad (25)$$

After solving for x (analogous to what we did for y), one obtains for the whole summation (18)

$$\begin{aligned} & \sum_{i=0}^{\eta} \sum_{j=0}^{\eta-i} \binom{\eta}{i} \binom{\eta-i}{j} v^i t^{\eta-i-j} u^j \frac{(-h(\nu))^{\delta + \frac{n+1}{2} + i + j}}{(\lambda - \nu)^{\delta+i+1} (-h(\lambda))^{\frac{n+1}{2} + j}} (x_{\max})^{\delta + \eta + \frac{l+n}{2} + 1} \\ & \times \frac{\Gamma(\eta + \frac{l+1}{2} - i - j) \Gamma(\frac{n+1}{2} + j) \Gamma(\delta + i + 1)}{\Gamma(\delta + \eta + \frac{l+n}{2} + 2)} \end{aligned} \quad (26)$$

The coefficients t , u and v are calculated by equalizing term by term in equation (17)

$$\begin{cases} \frac{1}{S_0 - S_{z_0}} = -t(\lambda + \gamma) + u(\nu + \gamma) + vq \\ 0 = -t + u + vs \\ -\frac{S_{z_0}}{S_0 - S_{z_0}} = t(\lambda + \gamma) \left[G(\lambda) - \frac{L_z^2}{2(\lambda + \alpha)} \right] - u(\nu + \gamma) \left[G(\nu) - \frac{L_z^2}{2(\nu + \alpha)} \right] + vrL_z^2 + vp \end{cases} \quad (27)$$

We find for the coefficients

$$v = \frac{v'}{x'_{\max}}, u = \frac{u'}{(\lambda - \nu)x'_{\max}}, t = \frac{t'}{(\lambda - \nu)x'_{\max}} \quad (28)$$

with

$$v' = \frac{\psi(\lambda, \nu) - S_{z_0} - \frac{L_z^2}{2\varpi^2}}{S_0 - S_{z_0}}, u' = -h(\lambda)v' - \frac{x'_{\max}}{S_0 - S_{z_0}}, t' = u' + s(\lambda - \nu)v' \quad (29)$$

Now we have a one-dimensional numerical integration to perform, like for the Abel components (Dejonghe & Laurent 1991).

4.3 The one-dimensional numerical integration

The triple integral (13) is reduced to a simple one if we judiciously choose the parameters p , q , r and s . The double integral in the (E, I_3) -plane (for a fixed L_z) can be solved analytically whenever $p + qE + rL_z^2 + sI_3 = 0$ does intersect the E -axis for $E \geq S_{z_0}(L_z)$. It has to be the case for all the L_z relevant in the integration. So if we take $p = -S_{z_0}$, $q = 1$ and $r \leq 0$, the double integral can be solved analytically because $E - S_{z_0} + rL_z^2 + sI_3 = 0$ intersects the E -axis for the value $E = S_{z_0} - rL_z^2 \geq S_{z_0}$. In that case, the double condition (9) becomes a simple one because the condition $E - S_{z_0} \geq 0$ is automatically verified when $E - S_{z_0} + rL_z^2 + sI_3 \geq 0$ since $s \leq 0$ and $I_3 \geq 0$.

We now have to determine the integration limits of the simple integral in L_z . Since conditions (1) and (9) imply that

$$S_{z_0}(L_z) \leq E \leq \psi - \frac{L_z^2}{2\varpi^2}, \quad (30)$$

the integration limits for the integral in L_z^2 are, in a first time, determined by the intersections of $S_{z_0}(L_z)$ and the line $E = \psi - \frac{L_z^2}{2\varpi^2}$ in the (E, L_z^2) -plane (see Figure 3).

Furthermore, in order to have a non-degenerate (i.e. not empty) triangle in Figure 2, we must have

$$x_{\max} \geq 0 \Leftrightarrow x'_{\max} \geq 0. \quad (31)$$

Since the condition $\psi - \frac{L_z^2}{2\varpi^2} - S_{z_0} \geq 0$ is automatically verified when condition (31) is verified, the equality in (31) fixes the minimal and maximal angular momentum to take into account in the integration.

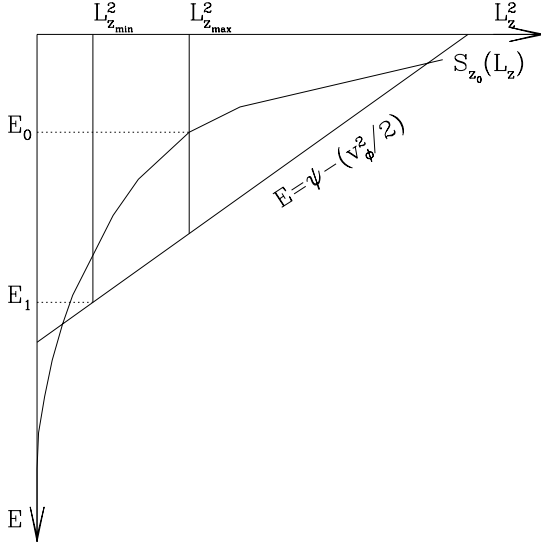


Figure 3. The (E, L_z^2) -plane. The integrations limits in L_z^2 , $(L_z^2)_{min}$ and $(L_z^2)_{max}$, must be between the intersections of the curve $E = S_{z_0}(L_z)$ and the line $E = \psi - \frac{v_\phi^2}{2}$. Condition (31) then definitively fixes these limits. E_0 and E_1 are the minimal and maximal energy taken into account in the integration.

Knowing that $L_z^2 = \varpi^2 v_\phi^2$, the resulting expression for the moment (with $a = 0$ and m even) becomes

$$\begin{aligned} \mu_{l,m,n} = & 2^{\frac{l+n}{2} + \beta + 1} \varpi^{2\beta} \frac{\Gamma(\delta + 1) \Gamma(\frac{n+1}{2}) \Gamma(\eta + \frac{l+1}{2})}{\Gamma(\delta + \eta + \frac{l+n}{2} + 2)} \int_{(v_\phi^2)_{min}}^{(v_\phi^2)_{max}} (v_\phi^2)^{\beta + \frac{m-1}{2}} (S_{z_0})^{\beta + \alpha_1} \frac{e^{-\frac{\alpha_2}{S_{z_0}}}}{2} \\ & \times \frac{(x'_{max})^{\delta + \frac{l+n}{2} + 1}}{(-h(\lambda))^{\frac{n+1}{2}} (-h(\nu))^{\eta + \frac{l+1}{2}}} \sum_{i=0}^{\eta} \sum_{j=0}^{\eta-i} \binom{\eta}{i} \binom{\eta-i}{j} v^i \\ & \times t'^{\eta-i-j} u'^j \frac{\Gamma(\delta + i + 1)}{\Gamma(\delta + 1)} \frac{\Gamma(\eta + \frac{l+1}{2} - i - j) \Gamma(\frac{n+1}{2} + j)}{\Gamma(\eta + \frac{l+1}{2}) \Gamma(\frac{n+1}{2})} \frac{(-h(\nu))^{i+j}}{(-h(\lambda))^j} dv_\phi^2 \end{aligned} \quad (32)$$

This integration has to be performed numerically.

In the general case $a \neq 0$, the expression (32) is still valid for the even moments. When m is odd, the integrandum has to be multiplied by a factor A :

$$A = \frac{1 - e^{-a\varpi|v_\phi|}}{1 + e^{-a\varpi|v_\phi|}} \quad (33)$$

5 PHYSICAL PROPERTIES OF THE COMPONENTS

In this section, we show the realistic disc-like character of our stellar distribution functions: their mass density has a finite extent in the vertical direction and an exponential decline in the galactic plane, they favour almost circular orbits and their velocity dispersions are different in the vertical and radial direction. By varying the parameters, we can give a wide range of shapes to the components.

In order to illustrate the role of the different parameters, we calculate the moments of many component distribution functions with different values for the parameters.

As galactic potential, we use one of the Stäckel potentials described by Famaey & Dejonghe (2001), that are extensions of the ones described by Batsleer & Dejonghe (1994). In the implementation of the theory we choose $p = -S_{z_0}$, $q = 1$, and $r = 0$.

5.1 The parameter z_0

This parameter was introduced in order to impose a maximum height above the galactic plane for the disc-like component (Figure 4): indeed, when $E \geq S_{z_0}$, an orbit cannot go higher than $z = z_0$, and the distribution function (8) is null for $E \leq S_{z_0}(L_z)$. In order to model samples of stars belonging to populations with different characteristic heights above the galactic plane, we can use a set of components with different values for this parameter.

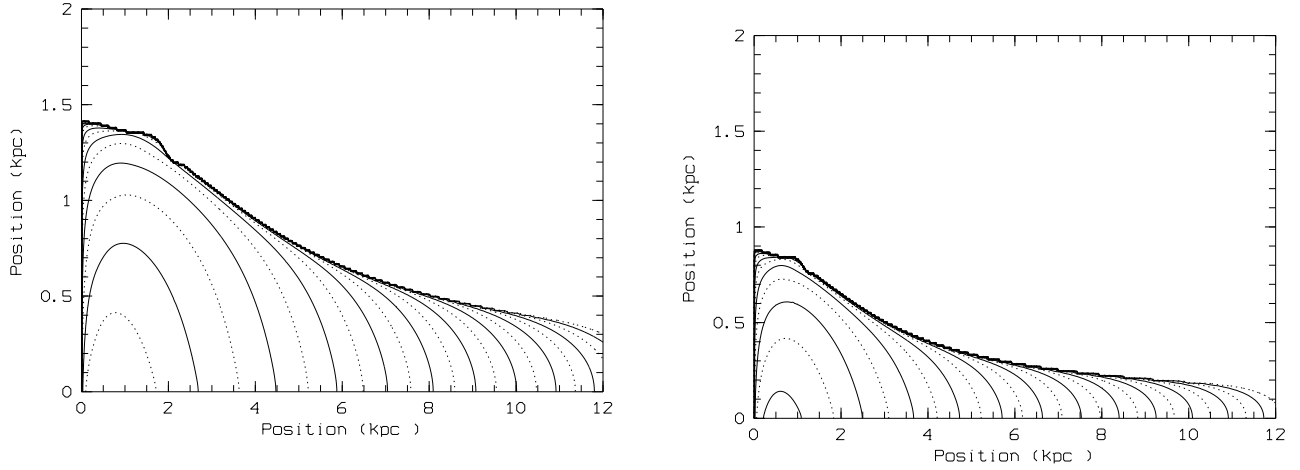


Figure 4. Contour plots of the mass density (i.e. the moment $\mu_{0,0,0}$) in a meridional plane, for components with the parameters $(\alpha_1, \alpha_2, \beta, \delta, \eta, z_0, s, a) = (3, 3, 1, 1, 2, z_0, -0.5, -5)$, with z_0 equal to 4 kpc (left panel) and 2 kpc (right panel) respectively (note the very different scale for ϖ and z). The discs become thinner with smaller z_0 , while the mass density is zero above $z = z_0$ (and even so below $z = z_0$ because $s \neq 0$). In this figure and in the following similar ones, every contour corresponds to a density that is a factor of 10 smaller than the next lower contour.

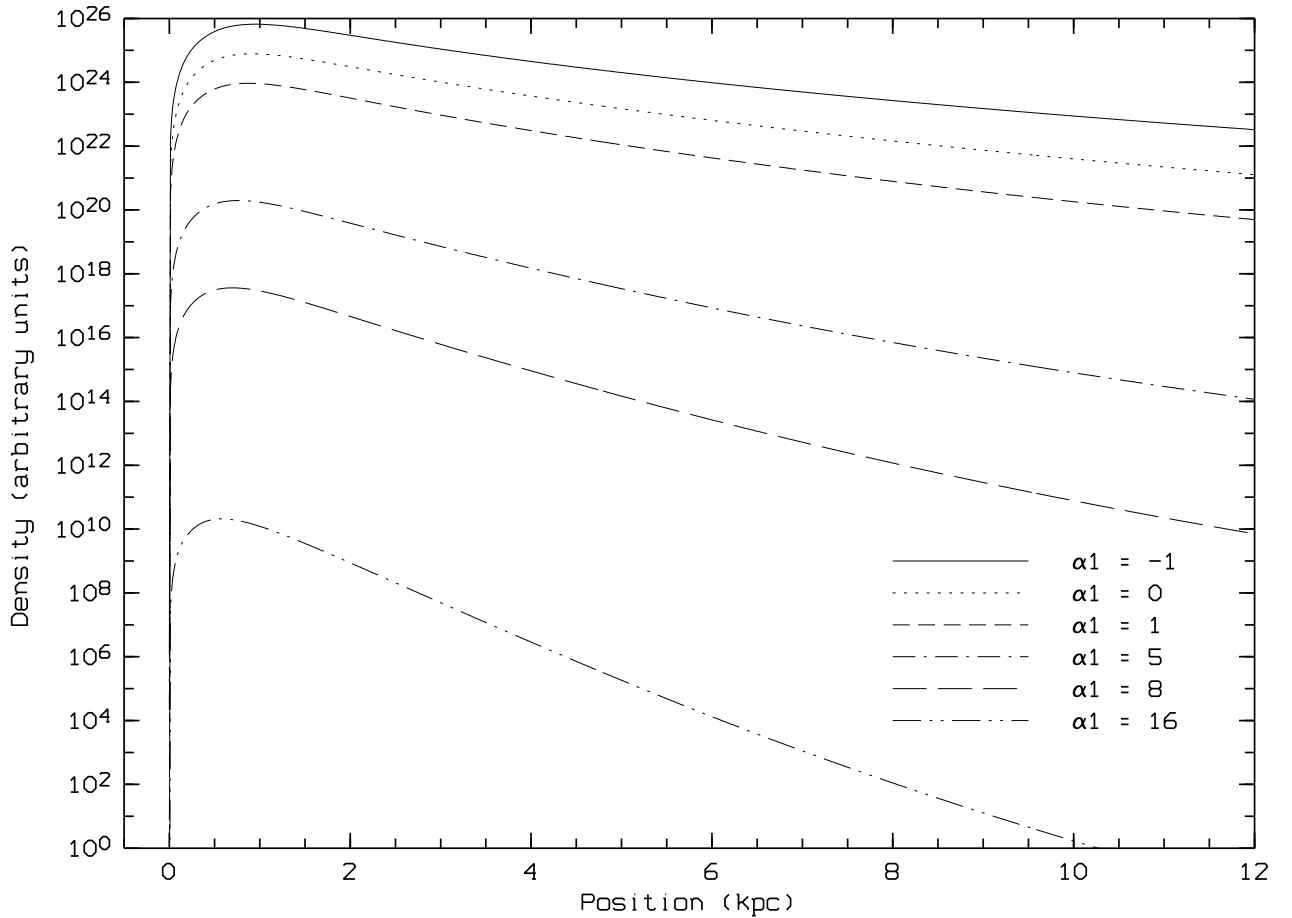


Figure 5. This figure displays the decline of the logarithm of the galactic plane mass density (in arbitrary units and scaling) of different components for varying α_1 . A rising α_1 helps to produce mass close to the center. The other parameters have the same values as in Figure 4 (with z_0 equal to 2 kpc) except that $\alpha_2 = 0$.

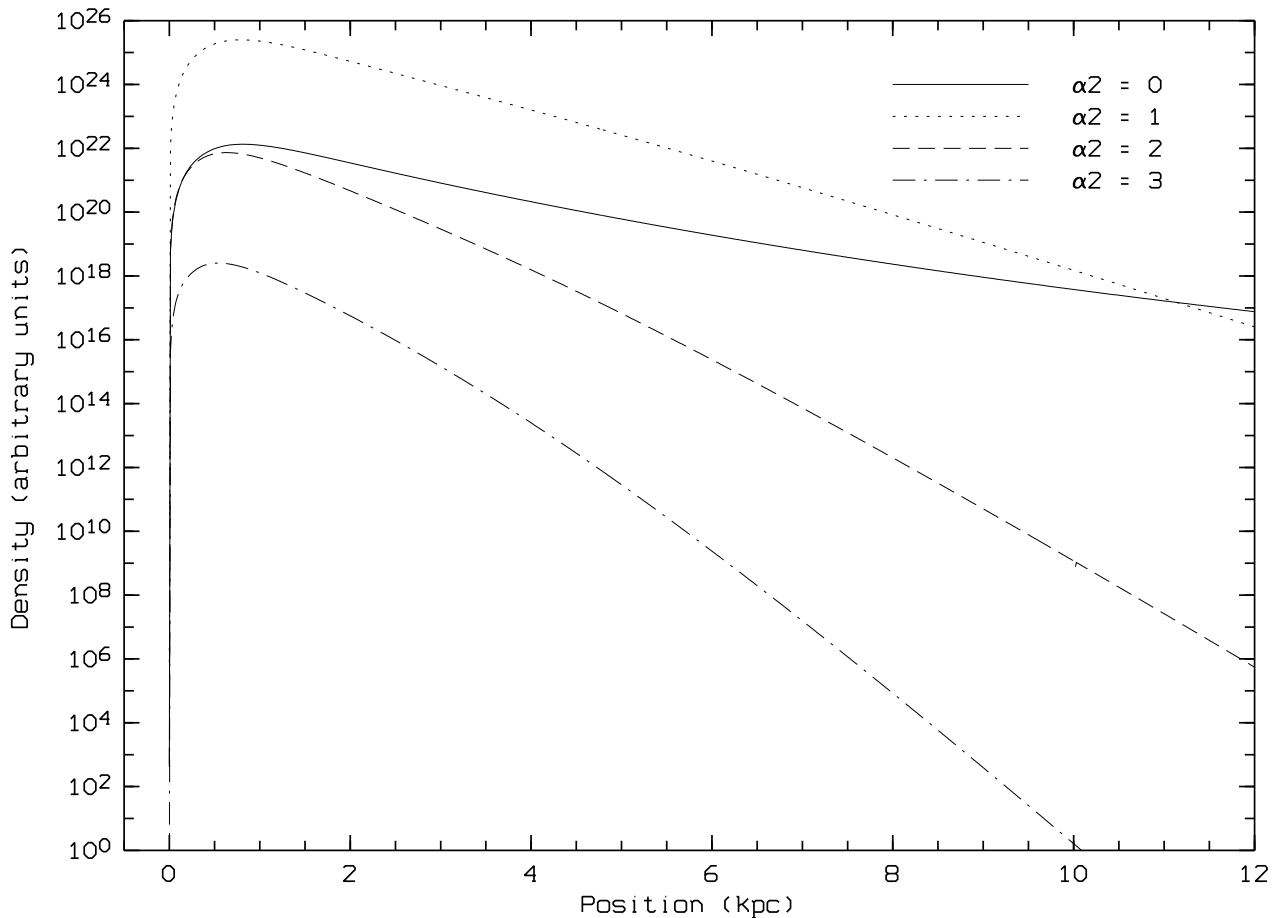


Figure 6. Logarithm of the configuration space density (in the galactic plane and in arbitrary units) of different components for varying α_2 . The other parameters have the same values as in Figure 4 (with z_0 equal to 2 kpc) except that α_1 is adjusted to built-in a given exponential decline. We see that the components have an exponential decline in the galactic plane and that α_2 is roughly the reciprocal of the component's scale length.

5.2 The parameter α_1

The parameter α_1 enters Eq. (10) as the exponent of S_{z_0} ; so, for non-negative values of α_1 , the factor where it appears will behave as a declining function of L_z , in the same way as $S_{z_0}(L_z)$ does, showing a steeper decline for larger α_1 (see Figure 5). A large α_1 thus results in a distribution function that favours a large fraction of bound orbits. When it is increasing, this parameter helps to produce mass close to the center.

When a given exponential decline is requested, α_1 will be a function of the other parameters rather than a fixed parameter (see section 5.3).

5.3 The parameter α_2

The parameter α_2 occurs as exponent in the distribution function's exponential factor. Increasing values of this parameter will contribute to the mass distribution near the center (Figure 6), like in the α_1 case (but exponentially).

On the other hand, our potential is approximately Keplerian at very large radii: this implies that, in the galactic plane,

$$L_z^2 \sim \varpi \quad (34)$$

and that (Batsleer & Dejonghe 1995)

$$S_{z_0}(L_z) \sim \frac{1}{L_z^2} \sim \frac{1}{\varpi} \quad (35)$$

So, at very large radii, α_2 is the reciprocal of the component's scale length, if the contribution of the other factors to the mass density does not vary much with respect to ϖ (for very large ϖ). In practice, it is often desirable to use components for which an exponential decline and a given scale length (as determined by α_2) is already built-in between two radii (say

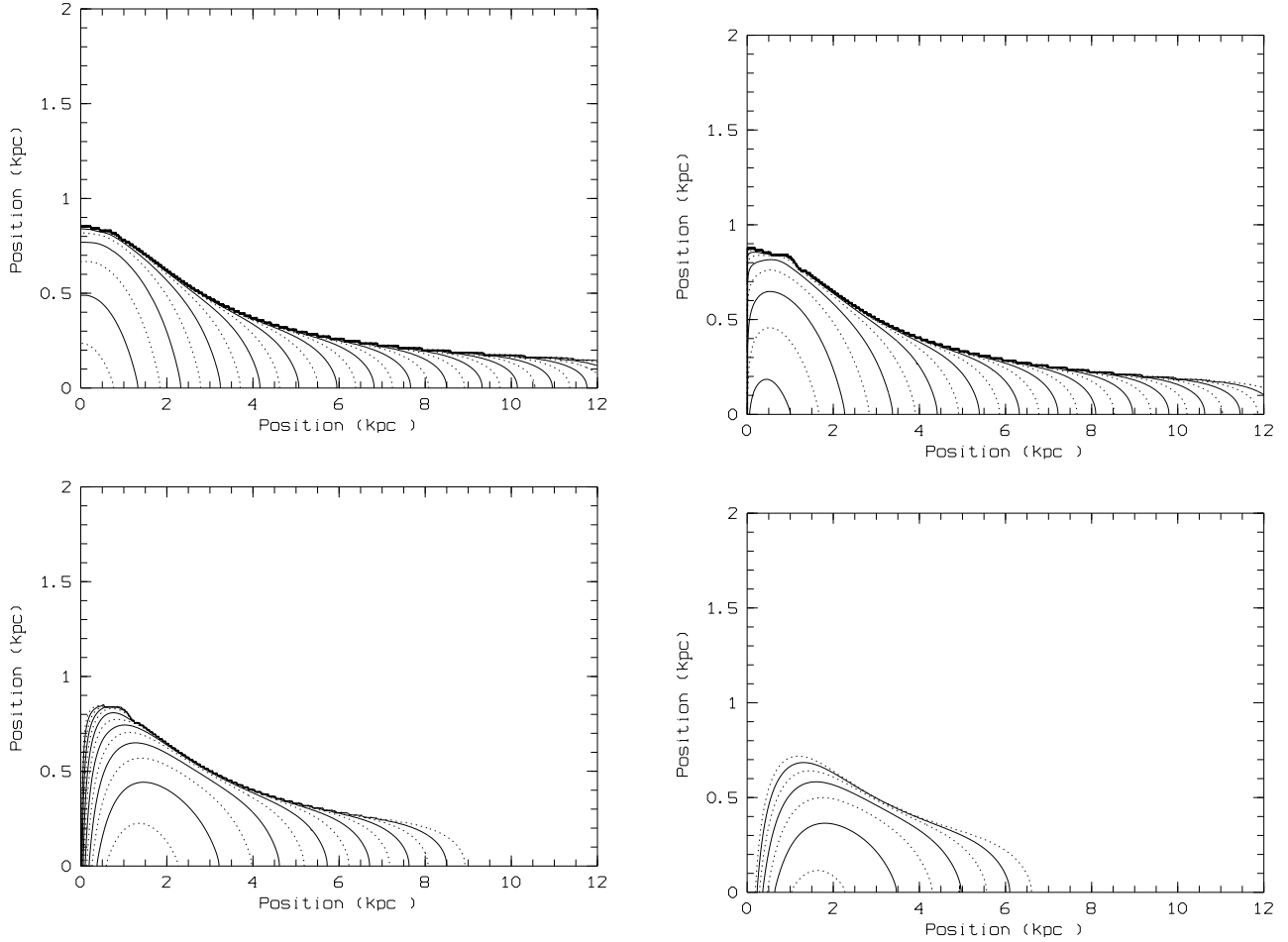


Figure 7. Contour plots of the configuration space density (the mass density) in a meridional plane, for components with the parameters $(\alpha_1, \alpha_2, \beta, \delta, \eta, z_0, s, a) = (3, 3, \beta, 1, 2, 2, -0.5, -5)$, with $\beta = 0$ (top left), $\beta = 0.5$ (top right), $\beta = 4$ (bottom left) and $\beta = 6$ (bottom right). We see that the maximum number of stars moves away from the center and that the mass is more concentrated in configuration space for an increasing β .

ϖ_1 and ϖ_2). In such cases, the parameter α_1 is adjusted in such a way that it corrects for the non-constant behaviour of the other factors at large radii, making the global contribution of all factors (except the one in α_2) constant at ϖ_1 and ϖ_2 .

5.4 The parameter β

For this parameter, there are two distinct cases: $\beta = 0$ and $\beta > 0$. In the first case, the density is maximum in the center and falls off smoothly. In the latter case, the density is null in the center since $L_z = 0$ for $\varpi = 0$. In order to model real stellar systems, we need components with $\beta = 0$ to have some mass in the center. However, in a real galaxy, the maximum number of stars occurs in the intermediate region where the bulge meets the disc: this justifies the utilization of components with $\beta > 0$ when modelling real stellar systems. We see the maximum density moving away from the center when β is rising (Figure 7).

We also see on Figure (7) that an increasing β will concentrate the mass in a smaller region of configuration space.

5.5 The parameter η

For a given L_z , the largest value of the factor $(E - S_{z_0})^\eta$ is obtained when the binding energy $E = S_0$ corresponds to the circular orbits in the galactic plane (see Figure 1). So, the parameter η is responsible for the favouring of almost circular orbits: a larger η implies a larger contribution of almost circular orbits (Figure 5.5) and thus a mass density located closer to the plane.

5.6 The parameter s

Condition (9) $E \geq S_{z_0} - sI_3$ implies that for $I_3 \neq 0$ and a strictly negative s , the orbits cannot reach the height z_0 above the galactic plane. We see on Figure (9) that the height z_0 is reached only in the case $s = 0$. Furthermore, since a large I_3

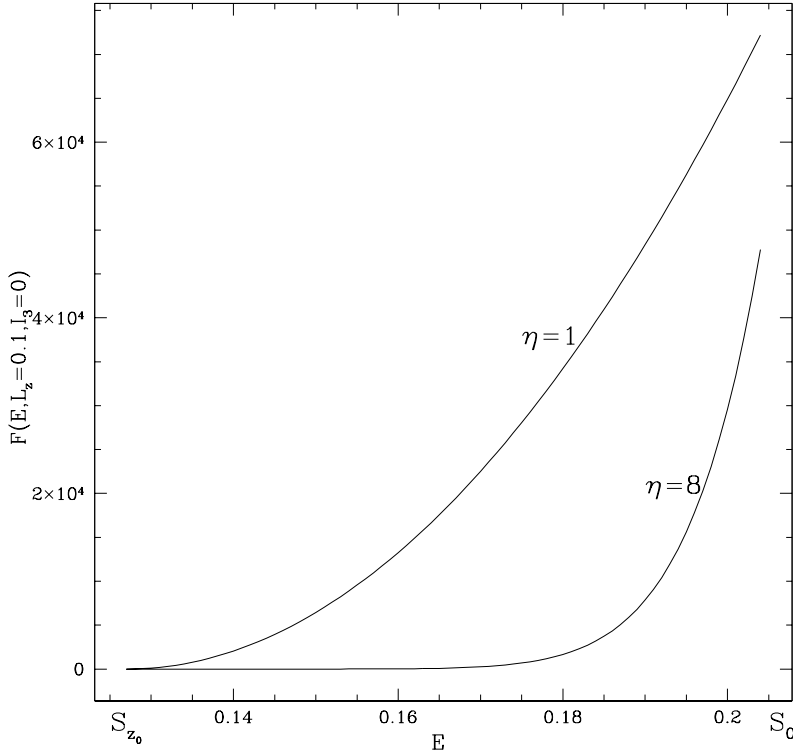


Figure 8. For $I_3 = 0$ and $L_z = 0.1$, this figure displays the value of a component distribution function (in arbitrary units) between $E = S_{z_0}$ and $E = S_0$ for $\eta = 1$ and $\eta = 8$. The other parameters have the same values as in Figure 4 (with z_0 equal to 2 kpc). We see that the proportion of circular orbits (close to $E = S_0$) is much higher for $\eta = 8$.

corresponds to an orbit that can reach a large height, the factor $(E - S_{z_0} + sI_3)^\delta$ favours orbits that stay low. So, by setting s more negative, we confine the orbits closer to the galactic plane.

A very important property of our components is the possibility of introducing a certain amount of anisotropy in the stellar disc: if we denote by σ_z the dispersion of the velocity in the direction perpendicular to the galactic plane, and by σ_ϖ the dispersion of the radial velocity in the galactic plane, then any nonzero s will produce a ratio $\frac{\sigma_z}{\sigma_\varpi}$ less than 1 (Figure 10). The ratio is closer to unity in the center than in the outer regions: this indicates the physically realistic character of our components. For $s = 0$, we find $\sigma_z = \sigma_\varpi$ since we are dealing with a two-integral component again.

5.7 The parameter δ

A large δ has partly the same effects as a large η : it favours circular orbits. Furthermore, a large δ augments the effects of the negative s and forces the stars to stay close to the plane by favouring low I_3 -values. As we can see on Figure (11), a component with a larger δ has more stars in the galactic plane but shows a steeper decline with respect to z .

6 MODELLING

The component distribution functions described in this paper are very useful as basis functions in the method described by Dejonghe (1989), in order to model any observable quantities (spatial mass density, velocity dispersions, average radial velocities on a sky grid,...). As an illustration, we present the application of the method to fit a given spatial density $\rho_0(\varpi, z)$ (see Batsleer & Dejonghe 1995 for a similar application in the two-integral approximation). We look for a linear combination of our components

$$\sum_{\Lambda} c_{\Lambda} F_{\Lambda} \quad (36)$$

that fits $\rho_0(\varpi, z)$, with $\Lambda = (\alpha_1, \alpha_2, \beta, \delta, \eta, z_0, s, a)$ and c_{Λ} the coefficients that are to be determined.

In practice, to find this linear combination we must introduce a grid (ϖ_i, z_i) in configuration space and minimize the quadratic function in c_{Λ} :

$$\chi^2 = \sum_i \left[\left(\sum_{\Lambda} c_{\Lambda} \mu_{0,0,0}^{(\Lambda)}(\varpi_i, z_i) \right) - \rho_0(\varpi_i, z_i) \right]^2 \quad (37)$$

This minimization, together with the constraint that the distribution function must be positive in phase space, is a problem of quadratic programming (hereafter QP) described by Dejonghe (1989).

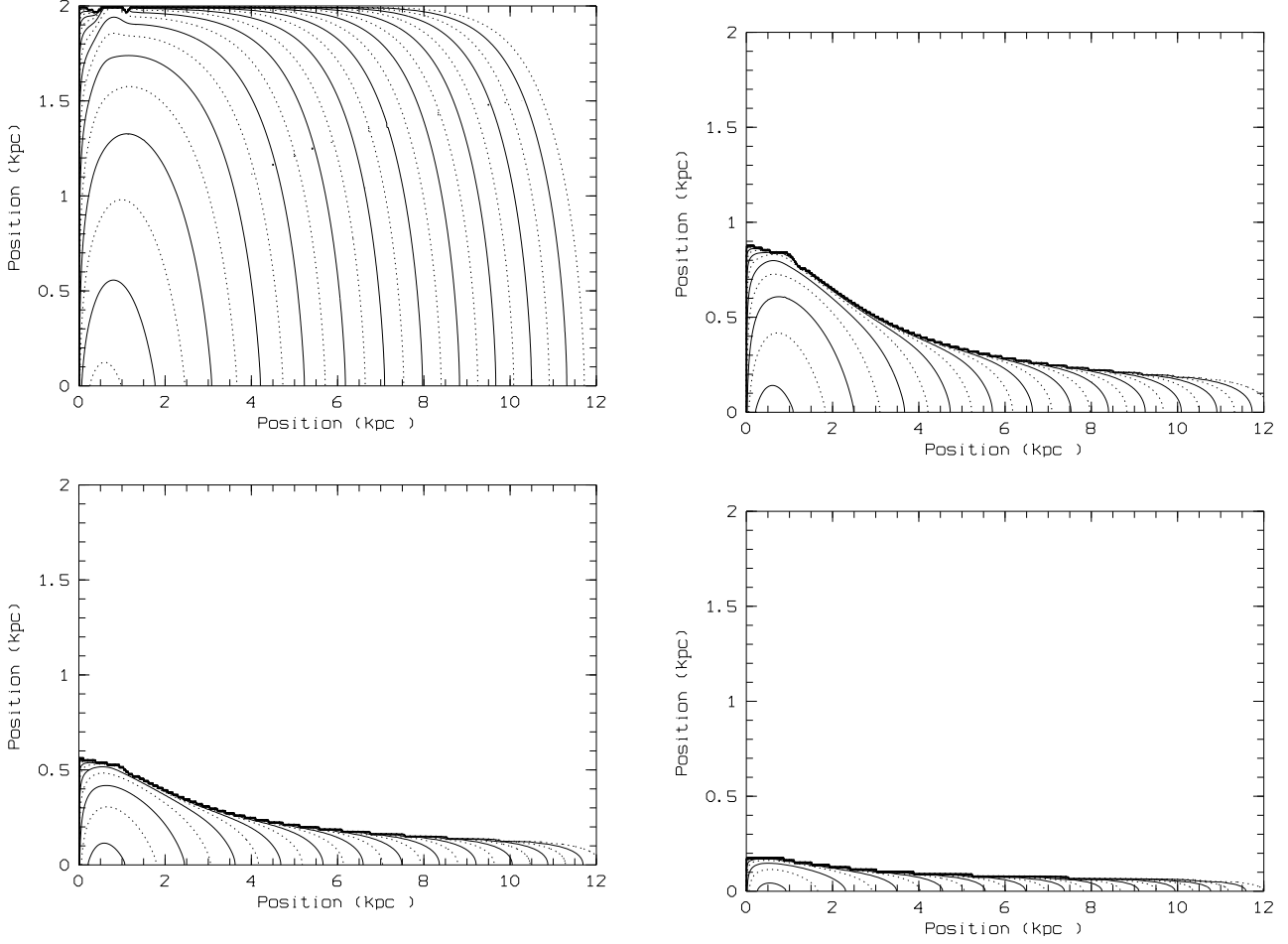


Figure 9. Contour plots of the configuration space density (the mass density) in a meridional plane, for components with the parameters $(\alpha_1, \alpha_2, \beta, \delta, \eta, z_0, s, a) = (3, 3, 1, 1, 2, 2, s, -5)$, with $s = 0$ (top left), $s = -0.5$ (top right), $s = -1$ (bottom left) and $s = -4$ (bottom right). The height z_0 is reached only in the case $s = 0$. The more negative s , the more the mass is concentrated near the galactic plane.

Here, we choose to adopt for ρ_0 a spatial density which closely resembles that of a real disc, i.e. a van der Kruit law, for which the vertical distribution is a good compromise between an exponential and an isothermal sheet (van der Kruit 1988).

$$\rho_0(\varpi, z) \propto \exp\left(-\frac{\varpi}{h_R}\right) \operatorname{sech}\left(\frac{z}{h_z}\right) \quad (38)$$

In order to have a zero derivative with respect to ϖ on the rotation axis, we adopt a mass density that follows closely the van der Kruit law, without a cusp in the center (see also Batsleer & Dejonghe 1995):

$$\rho_0(\varpi, z) = \frac{1 + 2\varpi/h_R}{1 + \varpi/h_R} \exp\left(-\frac{\varpi}{h_R}\right) \operatorname{sech}\left(\frac{z}{h_z}\right), \quad (39)$$

with h_R and h_z denoting the horizontal and vertical scale factor, respectively.

Since the moments $\mu_{0,0,0}$ are dependent on the potential of the galaxy (including the dark matter), we have to choose a potential for the galaxy that contains the stellar disc we want to model. We adopt a Stäckel potential with three mass components that produces a flat rotation curve and that therefore is a candidate potential for a disc galaxy (Famaey & Dejonghe 2001, see also Batsleer & Dejonghe 1994).

The actual modelling follows the same strategy as followed by Batsleer & Dejonghe (1995), which we briefly repeat here for easy reference. The first step in the actual modelling consists in the selection of a subset of components out of the (infinite) set of possible components. This subset is chosen so that certain features, that we suppose to be present in the stellar disc, such as circular orbits, are included. For example, we expect the mass density corresponding to a component to have an exponential behaviour close to the mass density we want to model. The QP program first minimizes the function (37) for one component F_λ and chooses the component of the initial subset that produces the lowest minimum for that function (37). Then the program iterates, selecting and adding at each iteration the component which, together with the components already chosen in a previous run, produces the best fit. Once the minimum of the χ^2 -variable does not change significantly any more with the addition of extra components, the program is halted because too low a value for χ^2 could imply that the QP program starts producing a distribution function featuring unnecessary oscillations.

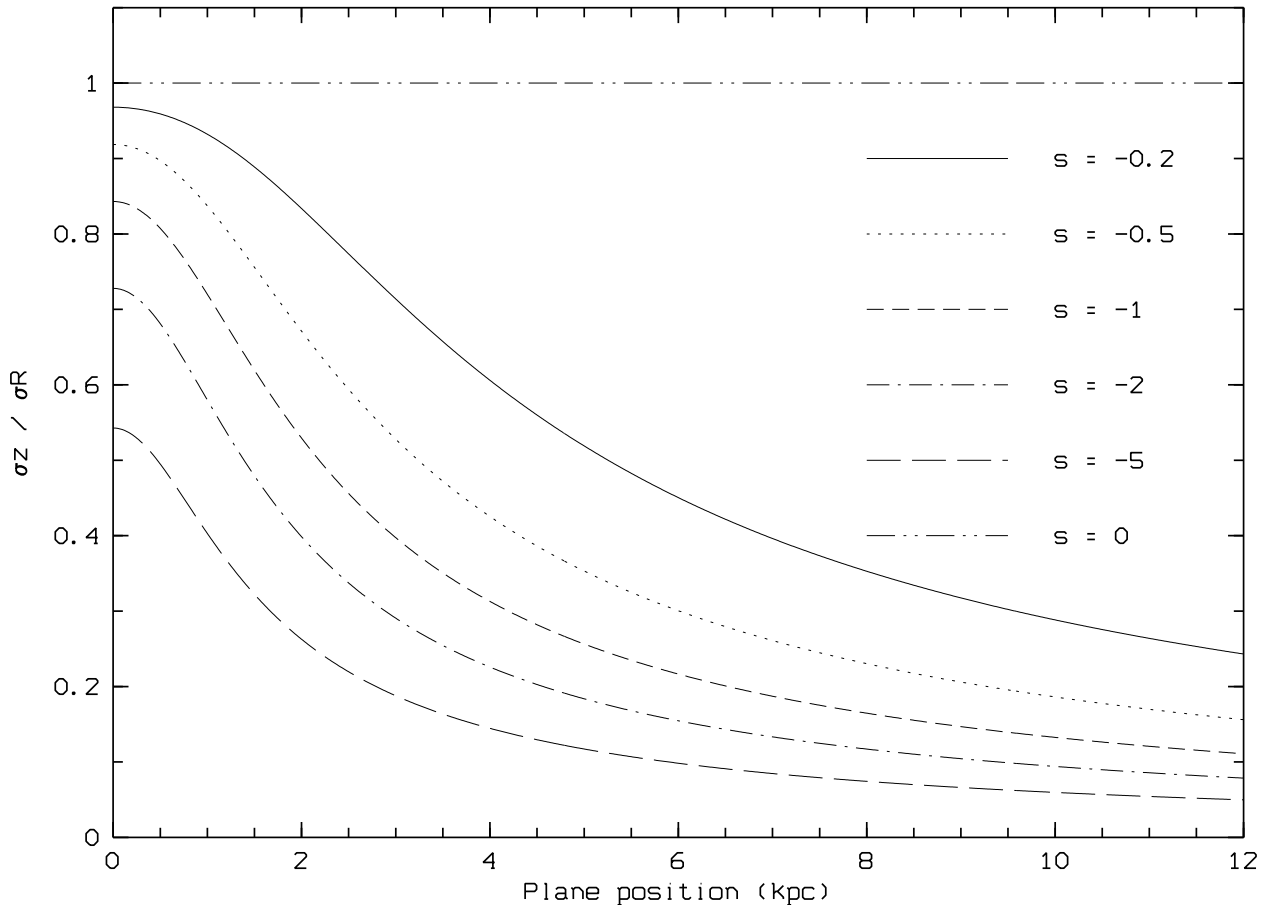


Figure 10. This figure displays the ratio $\frac{\sigma_z}{\sigma_w}$ of several components (in the Plane) for varying s . The other parameters have the same value as in Figure 9. The dependence of the components on the third integral induces anisotropy.

As an example, we model a modified van der Kruit disc with $h_R = 3\text{kpc}$ and $h_z = 0.25\text{kpc}$. Batsleer & Dejonghe (1995) already showed that a linear combination of two-integral components (with $s = 0$ and $\delta = 0$) could fit such a disc, but with $\sigma_w = \sigma_z$. In order to model real anisotropic velocity data in the future, the dependence on the third integral will be needed. We show that, by choosing components with $\beta = 0, 1, 3, 5, 7$; $\alpha_1 = 1$; $\alpha_2 = 0.15, 0.3, 2$; $z_0 = 1, 2, 4$; $\eta = 1, 5, 10$; $s = 0, -0.5, -1$; $\delta = 0.01, 1, 4$ and $a = 0$ in the initial subset, a fit with components featuring $s \neq 0$ and $\delta \neq 0$ can be obtained too (see Figure 12).

The fit is obtained for a linear combination of 25 components at 231 configuration space points (206 degrees of freedom). If we assume relative errors of 6%, we obtain for our minimum $\chi^2 = 246$, and the probability that a value of χ^2 larger than 246 should occur by chance is $Q(246/2, 206/2) \simeq 0.1$ (Abramowitz & Stegun 1972), which makes the goodness-of-fit believable (Press et al. 1986).

By using Stäckel dynamics to model a galactic disc, we construct a completely explicit and analytic distribution function, with an explicit dependence on the third integral. Figure (13) displays the distribution function obtained by QP in function of E , for $L_z = 0.1$ and for two values of I_3 ($I_3 = 0$ and $I_3 = 0.05$). For $I_3 = 0$, the distribution function is non-zero if $S_{z_0} \leq E \leq S_0$ (with $z_0 = 4\text{kpc}$); for $I_3 > 0$, instead, the maximum value of E is the one corresponding to infinitesimally thin short axis tubes and is smaller than S_0 . We see on Figure (13) that the distribution function is decreasing with increasing I_3 (particularly near $E = S_{z_0}$), and that it has some clumps. These clumps at $I_3 = 0.05$ are not discontinuities since the distribution function is a linear combination of continuous components.

Many different three-integral distribution functions correspond to a given spatial density, and there is no guarantee that they will yield realistic velocity dispersions. It is a major result of this paper to show that it is possible to find a linear combination of our components yielding realistic velocity dispersions. Figure (14) displays the ratio $\frac{\sigma_z}{\sigma_w}$ in the galactic plane: at the radius corresponding to the solar position in the Milky Way (7.5-8.5 kpc), the classical value of $\frac{\sigma_z}{\sigma_w} \simeq 0.4$ is obtained. The local maximum in the $\frac{\sigma_z}{\sigma_w}$ curve is due to the individual shapes of the velocity dispersions curves (Figure 14).

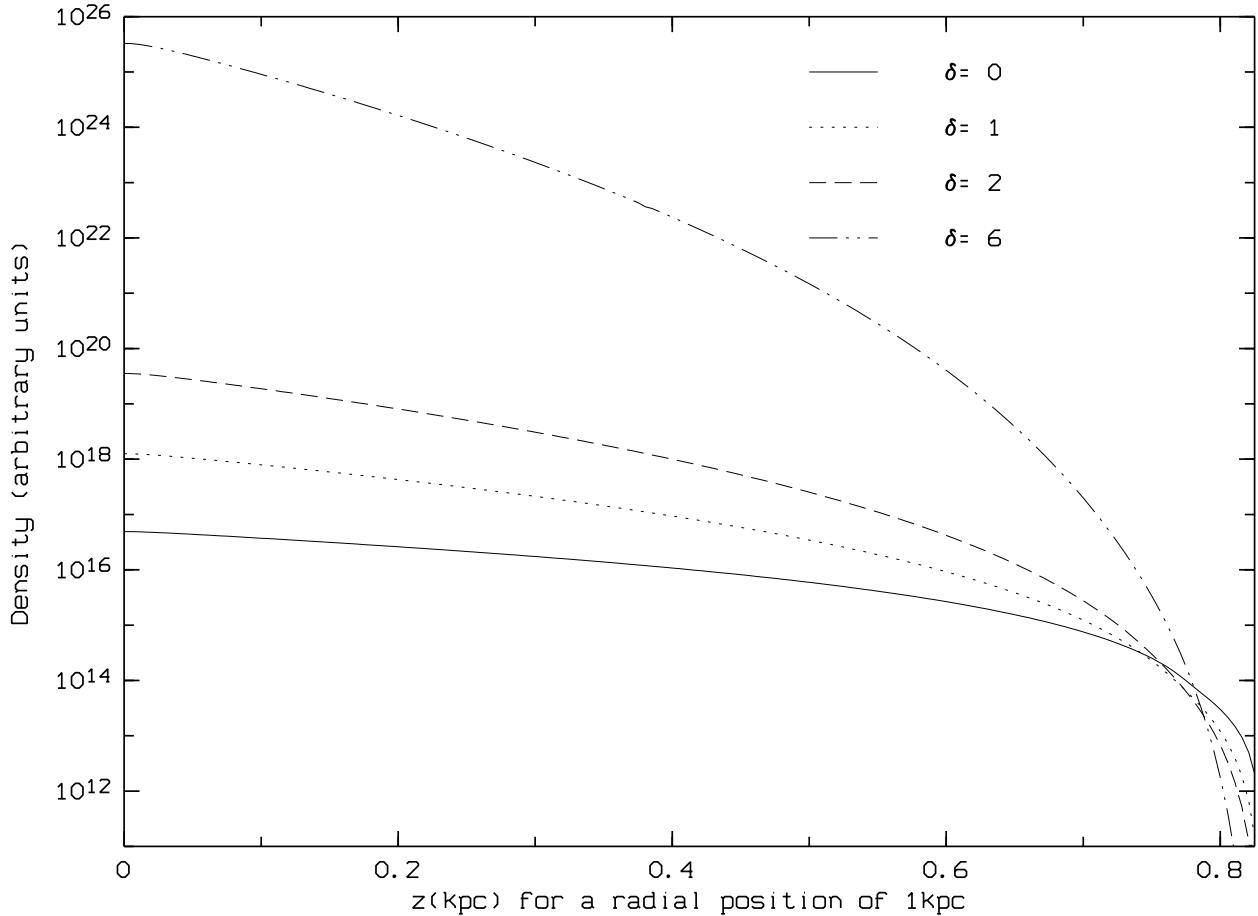


Figure 11. Decline of the logarithm of the configuration space density (in arbitrary units) as a function of the height above the Galactic plane at $\varpi = 1$ kpc for varying δ . A rising δ implies a steeper decline. The other parameters have the same values as in Figure 4 (with z_0 equal to 2 kpc).

7 CONCLUSIONS

In this paper, we have constructed new analytic three-integral stellar distribution functions yielding $\sigma_{\varpi} \neq \sigma_z$: they are generalizations of two-integral ones that can describe thin discs with the restriction that $\sigma_{\varpi} = \sigma_z$ (Batsleer & Dejonghe 1995).

We first reduced the triple integral defining their moments to a simple one, like in the Abel case (Dejonghe & Laurent 1991), by making some assumptions on the parameters. Then we looked for the effects of the different parameters and showed the disc-like (physically realistic) features of our distribution functions: they have a finite extent in vertical direction and an exponential decline in the galactic plane, while favouring almost circular orbits. A very important feature induced by the dependence on the third integral is their ability to introduce a certain amount of anisotropy, by varying the parameters responsible for this dependence (s and δ).

We finally showed that a van der Kruit disc can be modelled by a linear combination of such distribution functions with an explicit dependence on the third integral and a realistic anisotropy in velocity dispersions. This implies that they are very promising tools to model real data with $\sigma_{\varpi} \neq \sigma_z$ (Hipparcos data for example) by using the quadratic programming algorithm described by Dejonghe (1989). This will provide information on the dynamical state of tracer stars in the Milky Way (or on external galaxies).

ACKNOWLEDGEMENTS

We thank Dr Alain Jorissen very much for his permanent assistance. We thank the referee Dr Stephen Levine for his thorough reading of the manuscript and many helpful suggestions.

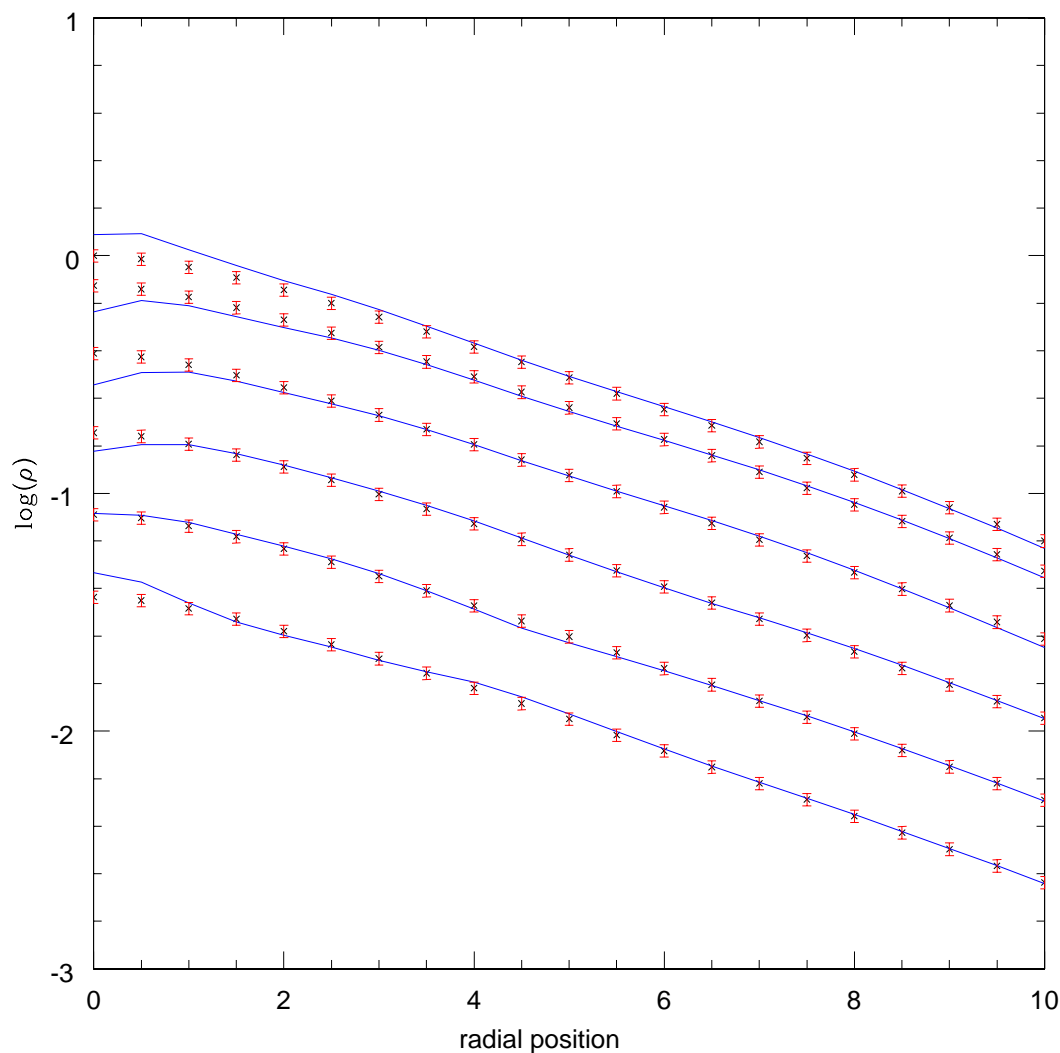


Figure 12. Data for a van der Kruit disc ($h_R = 3\text{kpc}$ and $h_z = 0.25\text{kpc}$) were generated in the region $0\text{ kpc} \leq \varpi \leq 10\text{ kpc}$ and $0\text{ kpc} \leq z \leq 1\text{ kpc}$. The initial subset of components was made of the components with $\beta = 0, 1, 3, 5, 7$; $\alpha_1 = 1$; $\alpha_2 = 0.15, 0.3, 2$; $z_0 = 1, 2, 4$; $\eta = 1, 5, 10$; $s = 0, -0.5, -1$; $\delta = 0.01, 1, 4$; $a = 0$. Components with non-zero s and non-zero δ were selected by the QP program. The crosses indicate the data for $z = 0\text{pc}, 200\text{pc}, 400\text{pc}, 600\text{pc}, 800\text{pc}, 1\text{kpc}$ (from top to bottom), with error bars. The solid lines correspond to the mass density of the components linear combination at these heights. The only region of our disc where the fit deviates a little from the data is the 2 kpc central region: our components are primarily intended to describe the outer regions rather than the central region of galaxies since most of them have a supermassive black hole at the center, sometimes associated with deviations from axisymmetry (bar).

REFERENCES

- Abramowitz M., Stegun I.A., 1972, Handbook of mathematical functions, Dover, New York
 Batsleer P., Dejonghe H., 1994, A&A, 287, 43
 Batsleer P., Dejonghe H., 1995, A&A, 294, 693
 Bienaymé O., 1999, A&A, 341, 86
 Bienaymé O., Séchaud N., 1997, A&A, 323, 781
 Binney J.J., Merrifield M.R., 1998, Galactic Astronomy, Princeton Univ. Press, Princeton
 Cretton N., de Zeeuw P.T., van der Marel R.P., Rix H.-W., 1999, ApJS, 124, 383
 Dehnen W.D., Gerhard O.E., 1993, MNRAS, 261, 311
 Dejonghe H., 1989, ApJ, 343, 113
 Dejonghe H., de Zeeuw P.T., 1988, ApJ, 333, 90
 Dejonghe H., Laurent D., 1991, MNRAS, 252, 606
 de Zeeuw P.T., 1985, MNRAS, 216, 273
 de Zeeuw P.T., Evans N.W., Schwarzschild M., 1996, MNRAS, 280, 903

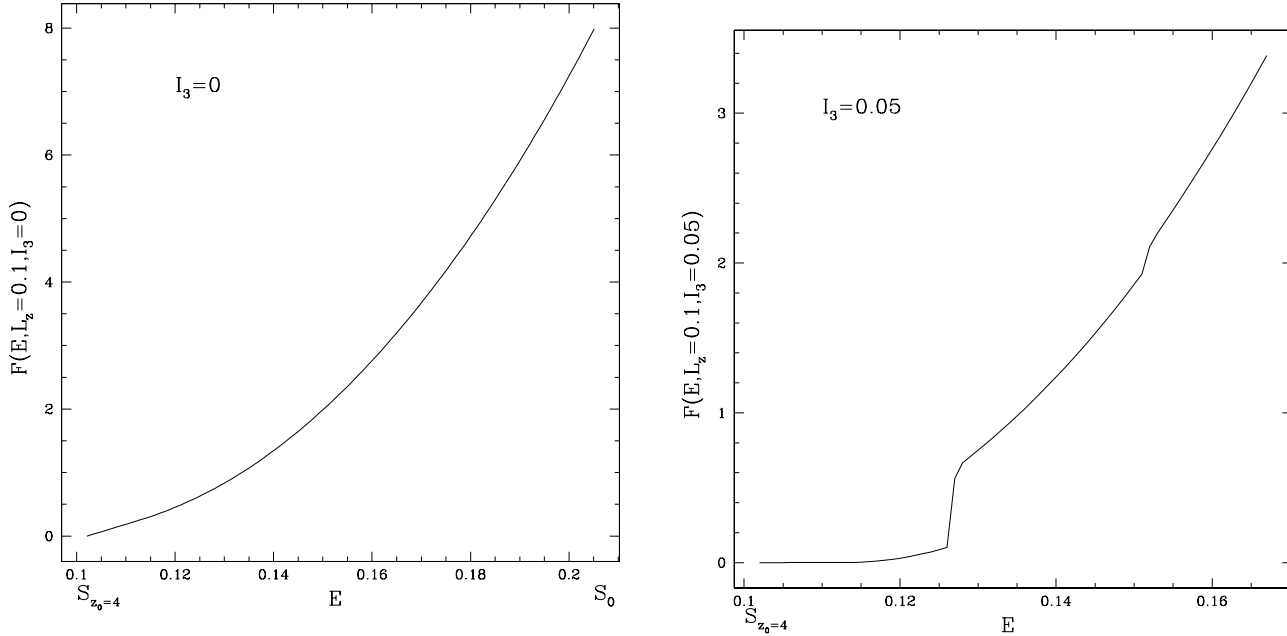


Figure 13. For $L_z = 0.1$ and a fixed I_3 (left panel: $I_3 = 0$, right panel: $I_3 = 0.05$), this figure displays the values of the distribution function (corresponding to the fit obtained in Figure 12) as a function of E (for the bound orbits). For $I_3 = 0.05$, the maximum value of E is the one corresponding to thin tube orbits and is smaller than S_0 .

- Durand S., Dejonghe H., Acker A., 1996, *A&A*, 310, 97
 Evans N.W., Häfner R., de Zeeuw P.T., 1997, *MNRAS*, 286, 315
 Famaey B., Dejonghe H., 2001, astro-ph/0112065
 Fricke W., 1952, *Astron. Nachr.*, 280, 193
 Häfner R., Evans N.W., Dehnen W.D., Binney J.J., 2000, *MNRAS*, 314, 433
 Innanen K.P., Papp K.A., 1977, *AJ*, 82, 322
 Jarvis B.J., Freeman K.C., 1985, *ApJ*, 295, 314
 Jeans J.H., 1915, *MNRAS*, 76, 70
 Kruit P.C. van der, 1988, *A&A*, 192, 117
 Ollongren A., 1962, *Bull. Astron. Inst. Netherlands*, 16, 241
 Petrou M., 1983a, *MNRAS*, 202, 1195
 Petrou M., 1983b, *MNRAS*, 202, 1209
 Press W.A., Flannery B.P., Teukolsky S.A., Vetterling W.T., 1986, *Numerical Recipes*, Cambridge Univ. Press, Cambridge
 Richstone D.O., 1982, *ApJ*, 252, 496
 Robijn F.H.A., de Zeeuw P.T., 1996, *MNRAS*, 279, 673
 Schwarzschild M., 1979, *ApJ*, 232, 236
 Stäckel P., 1890, *Math. Ann.*, 35, 91
 Zhao H.S., 1999, *CeMDA*, 73, 187

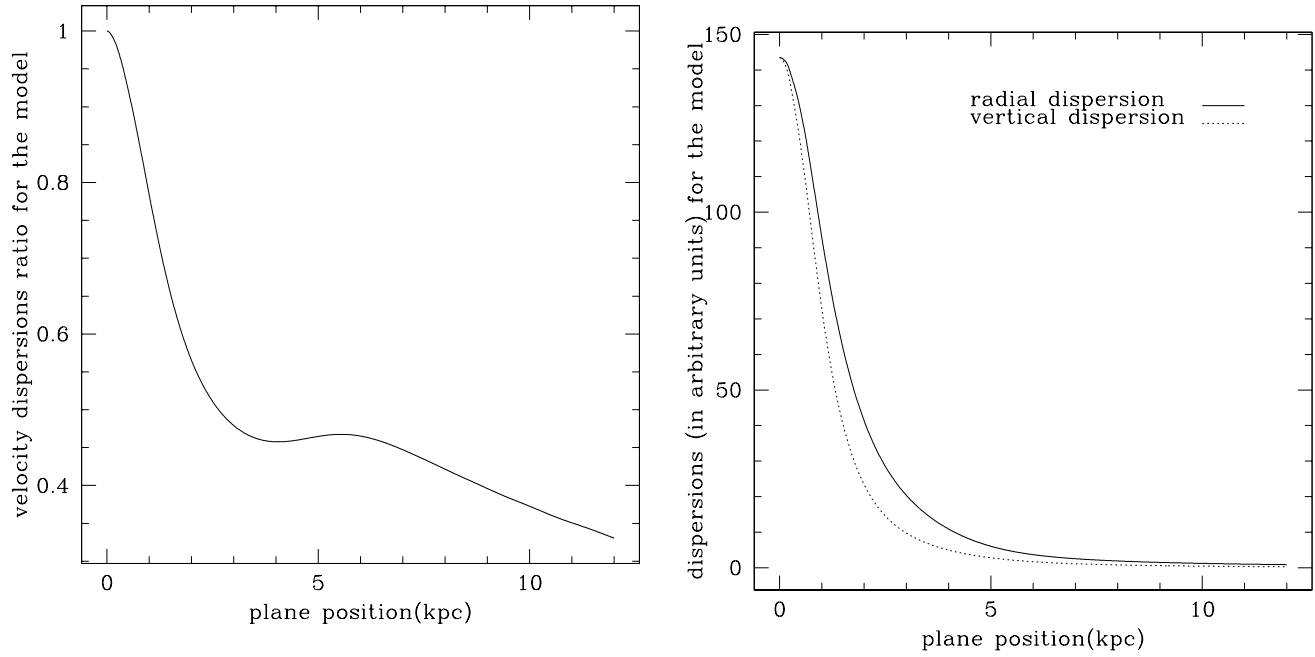


Figure 14. The left panel displays the ratio $\frac{\sigma_z}{\sigma_\varpi}$ in the galactic plane for the fit obtained in Figure 12. The right panel gives the shapes of the individual velocity dispersions curve σ_ϖ (solid line) and σ_z (dotted line) in the galactic plane.